

# Nanoparticle-Assisted Transcutaneous Delivery of a Signal Transducer and Activator of Transcription 3-Inhibiting Peptide Ameliorates Psoriasis-like Skin Inflammation

Jin Yong Kim,<sup>†,‡,⊥</sup> Jinhyo Ahn,<sup>§,||</sup> Jinjoo Kim,<sup>‡</sup> Minsuk Choi,<sup>‡</sup> Hyungsu Jeon,<sup>‡</sup> Kibaek Choe,<sup>§,||</sup> Dong Yun Lee,<sup>†,‡,⊥</sup> Pilhan Kim,<sup>§,||</sup> and Sangyong Jon<sup>\*,†,‡,⊥</sup>

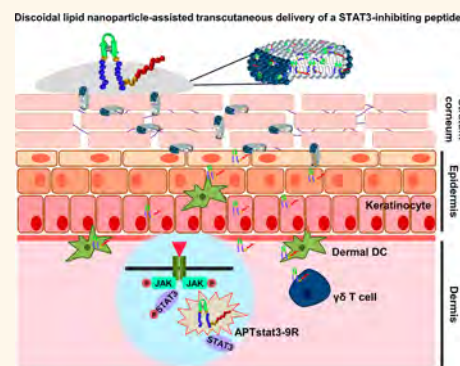
<sup>†</sup>Graduate School of Medical Science and Engineering, <sup>‡</sup>KAIST Institute for the BioCentury, Department of Biological Sciences, <sup>§</sup>Graduate School of Nanoscience and Technology, and <sup>||</sup>KAIST Institute for Health Science and Technology, Korea Advanced Institute of Science and Technology (KAIST), Daejeon 34141, Republic of Korea

<sup>⊥</sup>Division of Gastroenterology, Department of Internal Medicine and <sup>#</sup>Department of Nuclear Medicine, Asan Medical Center, University of Ulsan College of Medicine, Seoul 05505, Republic of Korea

## Supporting Information

**ABSTRACT:** Signal transducer and activator of transcription 3 (STAT3) is constitutively activated in psoriatic skin inflammation and acts as a key player in the pathogenesis and progression of this autoimmune disease. Although numerous inhibitors that intervene in STAT3-associated pathways have been tested, an effective, highly specific inhibitor of STAT3 has yet to be identified. Here, we evaluated the *in vitro* and *in vivo* biological activity and therapeutic efficacy of a high-affinity peptide specific for STAT3 (APTstat3) after topical treatment *via* intradermal and transcutaneous delivery. Using a preclinical model of psoriasis, we show that intradermal injection of APTstat3 tagged with a 9-arginine cell-penetrating peptide (APTstat3-9R) reduced disease progression and modulated psoriasis-related cytokine signaling through inhibition of STAT3 phosphorylation. Furthermore, by complexing APTstat3-9R with specific lipid formulations led to formation of discoidal lipid nanoparticles (DLNPs), we were able to achieve efficient skin penetration of the STAT3-inhibiting peptide after transcutaneous administration, thereby effectively inhibiting psoriatic skin inflammation. Collectively, these findings suggest that DLNP-assisted transcutaneous delivery of a STAT3-inhibiting peptide could be a promising strategy for treating psoriatic skin inflammation without causing adverse systemic events. Moreover, the DLNP system could be used for transdermal delivery of other therapeutic peptides.

**KEYWORDS:** signal transducer and activator of transcription 3, lipid nanoparticles, cell-penetrating peptide, aptides, psoriasis, transdermal delivery



Psoriasis is a common, chronic inflammatory skin disease affecting all ages that usually manifests as erythematous plaques with silvery scales.<sup>1</sup> Current estimates place the prevalence of psoriasis at up to 11.4% in adults.<sup>2</sup> Patients with psoriasis have a relapsing and remitting course during their lifetime that has a significant negative impact on quality of life. Psoriasis is characterized by epidermal hyperplasia, a result of hyperproliferation and aberrant differentiation of keratinocytes and massive infiltration of inflammatory immune cells. These cells crosstalk with each other through pro-inflammatory mediators, ultimately fueling a vicious cycle of psoriasis.<sup>3,4</sup>

Signal transducer and activator of transcription 3 (STAT3), a member of the STAT family, is activated by Janus kinase (JAK)-mediated phosphorylation, causing STAT3 to form

dimers that translocate into the nucleus, where they act as transcription factors.<sup>5</sup> STAT3 acts through regulation of numerous target genes to play an important role in cell survival, proliferation, differentiation, angiogenesis, and immune responses.<sup>6,7</sup> Notably, STAT3 is constitutively activated in epidermal keratinocytes of human psoriatic skin lesions.<sup>8</sup> Furthermore, STAT3 is critical for the differentiation of T-helper type 17 (T<sub>H</sub>17) cells and is an integral part of interleukin (IL)-6, IL-21, and IL-23 receptor signal trans-

Received: March 28, 2018

Accepted: June 21, 2018

Published: June 27, 2018

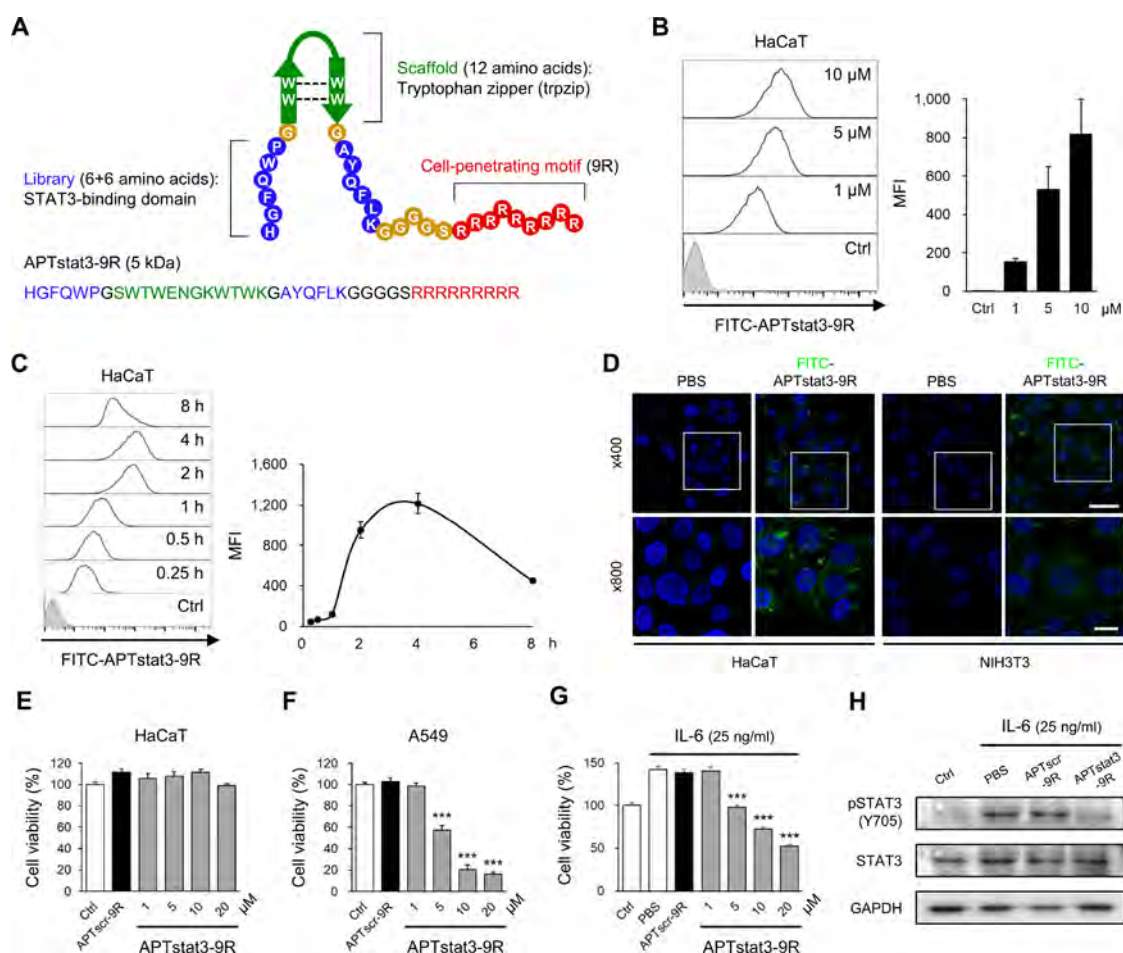


**Figure 1.** Biological activity APTstat3-9R in keratinocytes. (A) Schematic structure of APTstat3-9R. (B, C) Representative flow cytometry histogram of intracellular uptake of FITC-labeled APTstat3-9R into human keratinocytes. HaCaT cells were incubated with the indicated concentrations of FITC-labeled APTstat3-9R for 90 min (B) or with 10  $\mu\text{M}$  FITC-labeled APTstat3-9R for the indicated times (C). Shaded histograms represent negative controls. Graphs at right of histograms in (B) and (C) show quantification of FITC-labeled APTstat3-9R uptake in HaCaT cells as a function of APTstat3-9R concentration and time, respectively. MFI, mean fluorescence intensity. (D) Intracellular uptake and localization of FITC-labeled APTstat3-9R (10  $\mu\text{M}$ ) in HaCaT and NIH3T3 cells. Images were acquired by confocal microscopy at  $\times 400$  (top) and  $\times 800$  (bottom) magnifications. Scale bars, 50  $\mu\text{m}$  (top) and 20  $\mu\text{m}$  (bottom). (E–G) Viability of unstimulated HaCaT cells (E), A549 cells (F), and IL-6-stimulated HaCaT cells (G) following incubation with phosphate buffered saline (PBS), APTscr-9R (20  $\mu\text{M}$ ), or APTstat3-9R at the indicated concentrations for 24 h (unstimulated HaCaT cells) or 12 h (A549 cells and IL-6-stimulated HaCaT cells). The viability of aptide-treated cells was expressed as a percentage of control cell viability. (H) Western blot of pSTAT3 (Tyr705) and STAT3 in HaCaT cells pretreated with PBS, APTscr-9R (10  $\mu\text{M}$ ), or APTstat3-9R (10  $\mu\text{M}$ ) for 1 h and then stimulated with IL-6 (25 ng/mL) for 30 min pSTAT3, phosphorylated STAT3. Data are means  $\pm$  SEM of three independent experiments (\*\* $P < 0.001$ ; one-way ANOVA with *post hoc* Tukey test).

duction cascades, which expand and stabilize  $T_H17$  cells, thereby supporting their production of IL-17 and IL-22.<sup>9–12</sup> These previous studies clearly indicate that STAT3 is a key player in the development of psoriasis and an attractive target in the treatment of the disease. To date, a number of inhibitors against STAT3-associated pathways have been developed, including small molecules, decoy oligodeoxynucleotides, and peptides.<sup>7</sup> However, some inhibitors targeting upstream elements of STAT3 pathways, particularly JAKs, have been shown to cause severe adverse events because these kinases also phosphorylate a variety of proteins, including other STAT family members.<sup>13</sup> Given these limitations of existing STAT pathway inhibitors, there is a need to develop a STAT3 inhibitor that directly intervenes with only STAT3 phosphorylation without affecting JAKs.

Recent screening efforts using our aptide platform technology led to the identification of a high-affinity peptide

that specifically binds STAT3 (APTstat3), and our subsequent studies investigated the anticancer effect of APTstat3 tagged with a cell-penetrating 9-arginine peptide (APTstat3-9R) in various cancer models in which STAT3 is constitutively activated.<sup>14</sup> In the present study, we examined the suitability of APTstat3-9R as a topical therapeutic agent against psoriasis. Transcutaneous delivery is a favorable route for treating inflammatory skin diseases because it is simple, non-invasive, and avoids the risk of systemic side effects.<sup>15–17</sup> However, the formidable physiological barriers of the skin, particularly that posed by the stratum corneum (SC), hinder the penetration of hydrophilic or larger-sized molecules.<sup>18–20</sup> Although lipid-based formulations have been employed to enhance skin penetration of bioactive molecules,<sup>21–27</sup> their use in transdermal delivery of peptide therapeutics has been limited. Here, we report a discoid-shaped lipid nanoparticle (DLNP)-assisted transdermal system for delivery of APTstat3-9R and evaluated

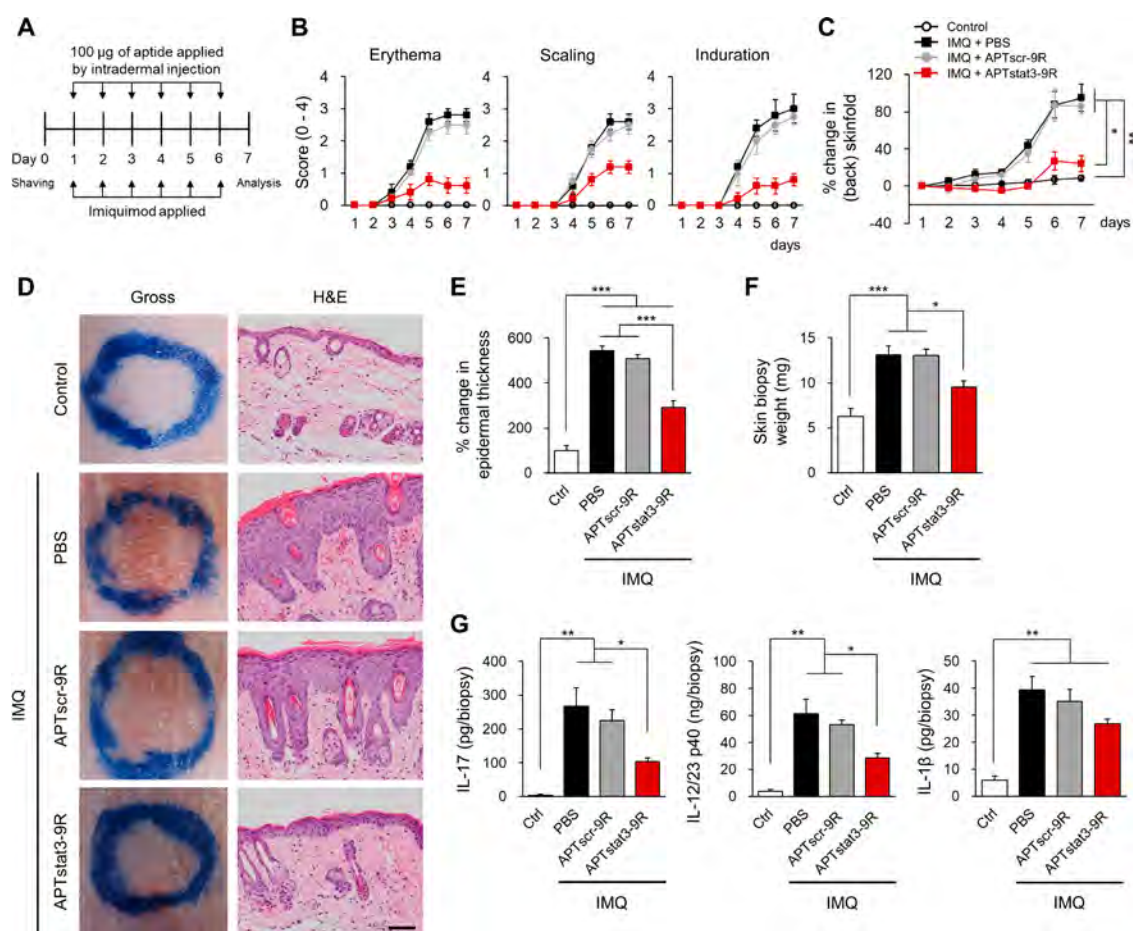


**Figure 2.** Intradermal administration of APTstat3-9R ameliorates psoriasis-like skin inflammation. (A) Experimental protocol for the murine model of imiquimod-induced psoriasis-like skin. Over the course of imiquimod application, a total of 100  $\mu\text{g}$  of APTscr-9R or APTstat3-9R, or an equivalent volume of PBS, was injected intradermally into the skin of the back for 6 days, as indicated. (B, C) Clinical parameters of disease severity were evaluated daily using a clinical scoring system based on the psoriasis area and severity index during the course of treatment. (B) Clinical score of skin erythema, scaling, and induration, and (C) back skinfold thickness. Skinfold thickness is expressed as a percentage relative to that in disease-free control mice. (D) Representative phenotypic presentation (left) and histological images of H&E staining (right) of mouse back skin after 6 days of treatment with PBS, APTscr-9R, or APTstat3-9R. Scale bar, 100  $\mu\text{m}$ . (E) Quantification of epidermal thickness. Values are percentages relative to disease-free controls. (F) Back skin punch biopsy weights. (G) Levels of inflammatory cytokines in skin homogenates. Data are presented as means  $\pm$  SEM ( $n = 5\text{--}6$  mice/group; \* $P < 0.05$ , \*\* $P < 0.01$ , and \*\*\* $P < 0.001$ ; one-way ANOVA with *post hoc* Tukey test). Ctrl, Vaseline-treated mice; IMQ, imiquimod-treated mice.

its therapeutic efficacy in a mouse model of psoriasis. We first demonstrate that intradermally injected APTstat3-9R attenuated psoriasis-like skin inflammation through suppression of STAT3 phosphorylation and inhibited the release of the key psoriasis-related cytokines, interleukin (IL)-23 and IL-17, in two different effector cell types. We further show that transcutaneously applied DLNPs containing APTstat3-9R successfully penetrated into the skin and ameliorated local psoriasis-like skin inflammation.

## RESULTS AND DISCUSSION

**APTstat3-9R Suppresses Proliferation of STAT3-Activated Keratinocytes through Inhibition of STAT3 Phosphorylation.** We previously showed that APTstat3-9R, whose sequence and molecular structure are shown in Figure 1A, selectively binds STAT3 and inhibits downstream signaling pathway in various cancer cells, thereby exerting anticancer efficacy in tumor-bearing mice.<sup>14</sup> Given the cell-penetrating properties of this STAT3 binder, we sought to determine whether APTstat3-9R can also be internalized by skin cells. To

this end, we incubated HaCaT human keratinocyte cells with different concentrations of fluorescein isothiocyanate (FITC)-labeled APTstat3-9R for various times and analyzed intracellular fluorescence using flow cytometry. As expected, intracellular fluorescence intensity gradually increased with increasing incubation time and APTstat3-9R concentration (Figure 1B, C), reaching a maximum at 4 h. FITC-labeled APTstat3-9R was distributed to both cytoplasmic and nuclear compartments of HaCaT cells; a similar pattern of cellular uptake was seen in NIH3T3 murine fibroblasts (Figure 1D).

Next, we evaluated the cytotoxicity of APTstat3-9R in HaCaT and NIH3T3 cells. A scrambled aptide (APTscr-9R), with the same scaffold but containing target-binding regions consisting of a scrambled sequence, was used as a control.<sup>14</sup> Treatment with APTstat3-9R for 24 h did not adversely affect the viability of keratinocytes or fibroblasts (Figure 1E and Figure S1). In contrast, treatment of human lung carcinoma cells (A549), which constitutively express activated STAT3, with APTstat3-9R (10–20  $\mu\text{M}$ ) caused nearly a complete loss of cell viability; as expected, the negative control, APTscr-9R

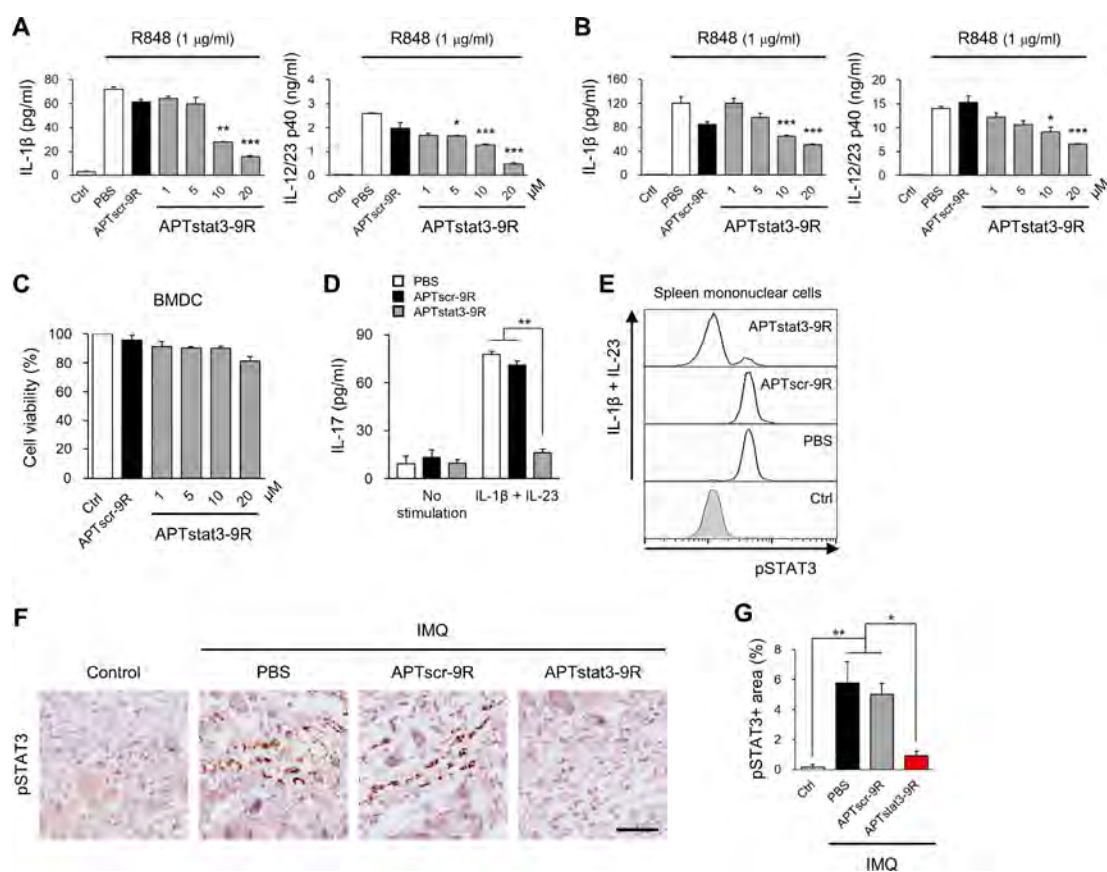


**Figure 3.** APTstat3-9R attenuates psoriasis-related cytokine production *in vitro* and *in vivo* through inhibition of STAT3 phosphorylation. (A, B) Cytokine production by BMDCs (A) and BMDMs (B) pretreated with PBS or the indicated concentrations of APTscr-9R (20 μM) or APTstat3-9R for 6 h, followed by stimulation with R848 (1 μg/mL) for 18 h. (C) Viability of unstimulated BMDCs, incubated with PBS or the indicated concentrations of APTscr-9R (20 μM) or APTstat3-9R for 24 h. The viability of aptide-treated cells was expressed relative to that of control cell viability as a percentage. (D) IL-17 production by γδ-T cells pretreated with PBS, APTscr-9R (10 μM), or APTstat3-9R (10 μM) for 4 h, followed by stimulation with IL-1β (10 ng/mL) and IL-23 (50 ng/mL) for 12 h. Cytokine levels in culture supernatants for experiments shown in (A, B, D) were determined by ELISA. (e) Representative flow cytometry histogram of pSTAT3 in isolated splenic mononuclear cells pretreated with PBS, APTscr-9R (10 μM), or APTstat3-9R (10 μM) for 1 h and then stimulated with IL-1β (10 ng/mL) and IL-23 (50 ng/mL) for 30 min. Shaded histograms represent negative controls. Data in (A–E) represent the average of three independent experiments. (F) Representative immunohistochemical staining for pSTAT3 in skin lesions in the imiquimod-induced psoriatic mouse model after 6 days of treatment with PBS, APTscr-9R, or APTstat3-9R. Scale bar, 100 μm. (G) Quantification of immunohistochemical staining for pSTAT3. pSTAT3-positive areas are expressed as a percentage of the total psoriatic skin lesion area ( $n = 5$  mice/group). Data are presented as means  $\pm$  SEM (\* $P < 0.05$ , \*\* $P < 0.01$ , and \*\*\* $P < 0.001$ ; one-way ANOVA with *post hoc* Tukey test). pSTAT3, phosphorylated STAT3.

(20 μM), had no effect on the viability of either cell type (Figure 1E, F). Interestingly, in HaCaT keratinocytes that had been stimulated with IL-6 (25 ng/mL), a major activator of STAT3 signaling, APTstat3-9R caused a concentration-dependent reduction in cell proliferation (Figure 1G). Moreover, whereas STAT3 was rapidly phosphorylated in IL-6-stimulated keratinocytes, this activating phosphorylation was blocked by APTstat3-9R (10 μM), as shown by Western blot analysis (Figure 1H). These findings suggest that APTstat3-9R is internalized into normal keratinocytes and fibroblasts without substantially affecting their viability, but suppresses proliferation of STAT3-activated keratinocytes by inhibiting phosphorylation of STAT3.

**Intradermal Injection of APTstat3-9R Ameliorates Psoriasis-like Skin Inflammation.** To investigate the biological activity of APTstat3-9R against psoriasis-like skin inflammation, we first tested an intradermal injection route. A mouse model of psoriasis was established by topical treatment of the whole back of mice for 6 consecutive days with

imiquimod cream, a Toll-like receptor (TLR)-7 and -8 agonist. After exposure to cream for 2 h, mice were intradermally injected twice a day at a 4 h interval at the indicated area of the back with APTstat3-9R (50 μg) and sacrificed on day 7 (Figure 2A). Disease severity was evaluated daily using an objective scoring system based on the Psoriasis Area and Severity Index (PASI). APTstat3-9R treatment ameliorated the severity of clinical signs, including erythema, scaling, induration, and skinfold thickness, at the site of injection compared with PBS or APTscr-9R from days 5 to 7 (Figure 2B,C). Consistent with clinical scores, gross findings were also improved (Figure 2D). Furthermore, histological analyses of punch biopsy specimens from the back skin of APTstat3-9R-treated mice showed a considerable reduction in epidermal hyperplasia and inflammatory cell infiltration compared with mice treated with PBS or APTscr-9R (Figure 2D,E). These findings were further supported by the reduced weight of punch biopsy specimens (Figure 2F), suggesting a reduction in skin edema in APTstat3-9R-treated mice compared with

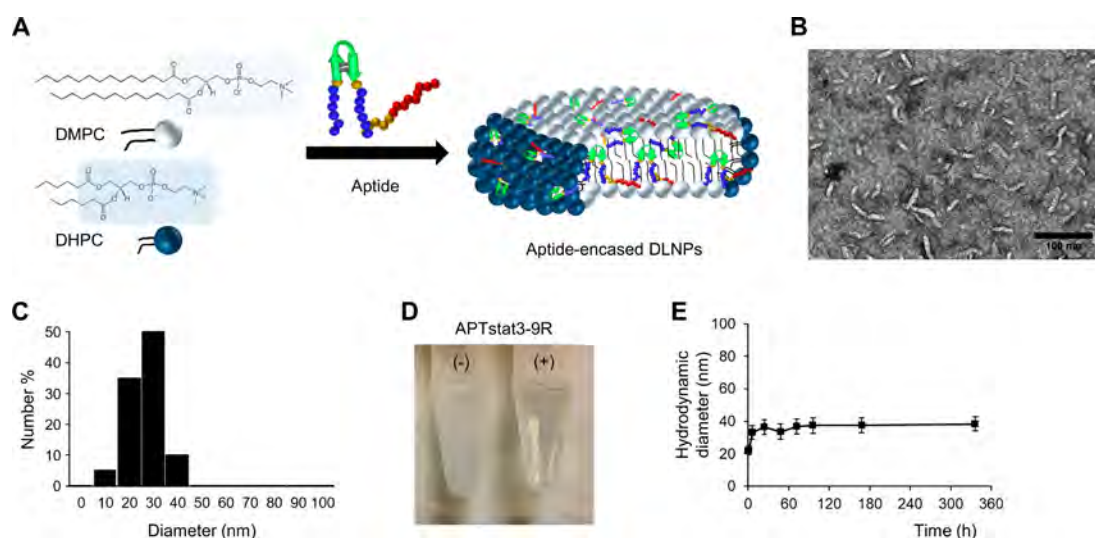


**Figure 4.** Characterization of aptide-encased, discoid-shaped lipid nanoparticles. (A) Schematic representation of aptide-encased, discoid-shaped lipid nanoparticles (DLNPs) consisting of long-chain phospholipid (DMPC) and short-chain phospholipid (DHPC) containing APTstat3-9R. APTstat3-9R was added a concentration of 10 wt % to a lipid mixture containing a DMPC/DHPC molar ratio of 3:1. (B) Representative TEM image of [APTstat3-9R]-DLNPs. Scale bar, 100 nm. (C) Histogram showing the particle size distribution of [APTstat3-9R]-DLNPs, based on a TEM analysis of 200 nanostructures. (D) Photograph of tubes containing DLNPs without (–) and with (+) APTstat3-9R 6 h after preparation. (E) The stability of [APTstat3-9R]-DLNPs in distilled water at ambient temperature over time, as analyzed by dynamic light scattering. Data are presented as means  $\pm$  SD.

controls. Moreover, protein levels of the psoriasis-related cytokines, IL-17, IL-12/23p40, and IL-1 $\beta$ , in skin homogenates were significantly reduced by treatment with APTstat3-9R (Figure 2G). Notably, psoriasis model mice in all groups (PBS, APTstat3-9R, APTscr-9R) showed typical adverse systemic effects of the TLR agonist, including weight loss, apathetic behavior, and splenomegaly (Figure S2), during the experimental period compared with controls that had not been topically treated with imiquimod cream. Collectively, these results indicate that APTstat3-9R effectively ameliorates local psoriasis-like skin inflammation upon intradermal injection, but it does not affect systemic adverse events induced by imiquimod cream.

**APTstat3-9R Attenuates Production of Psoriasis-Related Cytokines by Inhibiting STAT3 Phosphorylation.** It has been shown that, during the initiation of psoriasis, both dendritic cells and macrophages are activated by TLR7, -8, or -9 and subsequently produce the proinflammatory cytokines, IL-1 $\beta$ , IL-12, and IL-23, which polarize naive T cells into IL-17-producing T cells.<sup>3,28,29</sup> Accordingly, we next investigated the effects of APTstat3-9R on psoriasis-related cytokine signaling in these effector cell types after stimulation with a TLR7 ligand. Accordingly, mouse bone marrow-derived dendritic cells (BMDCs) and macrophages (BMDMs) were stimulated with R848 (1  $\mu$ g/mL), a dual TLR7 and -8 agonist, in the presence of APTstat3-9R or APTscr-9R. As expected, APTscr-9R had no effect on cytokines; in contrast, incubation with APTstat3-9R for 18 h significantly reduced the production of IL-1 $\beta$  and IL-12/23p40 in R848-stimulated BMDCs in a concentration-dependent manner (Figure 3A), but had no effect on BMDC viability (Figure 3C). A similar trend was observed in BMDMs cultured under the same conditions (Figure 3B). These data indicate that APTstat3-9R reduces TLR7-induced proinflammatory cytokine production in both effector cell types without affecting cell viability.

Because the IL-23/IL-17 axis is a major pathogenic pathway in psoriasis during the chronic phase,<sup>3,11</sup> we next investigated

the effect of APTstat3-9R on the production of IL-17 in  $\gamma\delta$ -T cells. Since previous studies have demonstrated that  $\gamma\delta$ -T cells produce IL-17 in response to IL-1 $\beta$  and IL-23 in the absence of T-cell receptor engagement,<sup>12,30</sup> we did not use an anti-CD3e antibody in these experiments. The  $\gamma\delta$ -T cells isolated from mouse spleen and draining lymph nodes were pretreated with APTstat3-9R (10  $\mu$ M) for 4 h, followed by stimulation with IL-1 $\beta$  (10 ng/mL) and IL-23 (50 ng/mL) for an additional 12 h, after which secreted IL-17 protein was quantified. Notably, APTstat3-9R suppressed IL-17 production by IL-1 $\beta$ /IL-23-stimulated  $\gamma\delta$ -T cells, whereas APTscr-9R did not (Figure 3D). We next examined whether APTstat3-9R inhibited phosphorylation of STAT3 in cytokine-stimulated  $\gamma\delta$ -T cells. After pretreating murine splenic mononuclear cells with APTstat3-9R or APTscr-9R (10  $\mu$ M) for 1 h and subsequently stimulating with IL-1 $\beta$  and IL-23 for 30 min, we analyzed STAT3 phosphorylation by flow cytometry. As shown in Figure 3E, unlike APTscr-9R, APTstat3-9R effectively suppressed STAT3 phosphorylation compared with PBS-treated control cells, suggesting that APTstat3-9R effectively inhibits key signaling pathways associated with psoriasis pathogenesis. We further performed immunohistochemical analyses for phosphorylated STAT3 (pSTAT3) in the imiquimod-induced psoriasis mouse model. As seen in images of the upper dermis of psoriatic skin, pSTAT3 immunostaining was markedly reduced in APTstat3-9R-treated mice compared to that in PBS- or APTscr-9R-treated mice (Figure 3F,G). Immunostaining for IL-17 yielded similar results (Figure S3). Collectively, these findings clearly suggest that APTstat3-9R is able to reduce production of psoriasis-related cytokines by inhibiting STAT3 phosphorylation *in vitro* as well as *in vivo*.

**Preparation and Characterization of APTstat3-9R-Encased DLNPs.** Although topical application is a convenient and effective route for administering therapeutics for early to mild psoriatic skin, transcutaneous delivery of peptide-based therapeutics has been a more challenging proposition. When applied topically to imiquimod-induced psoriasis-like skin of a

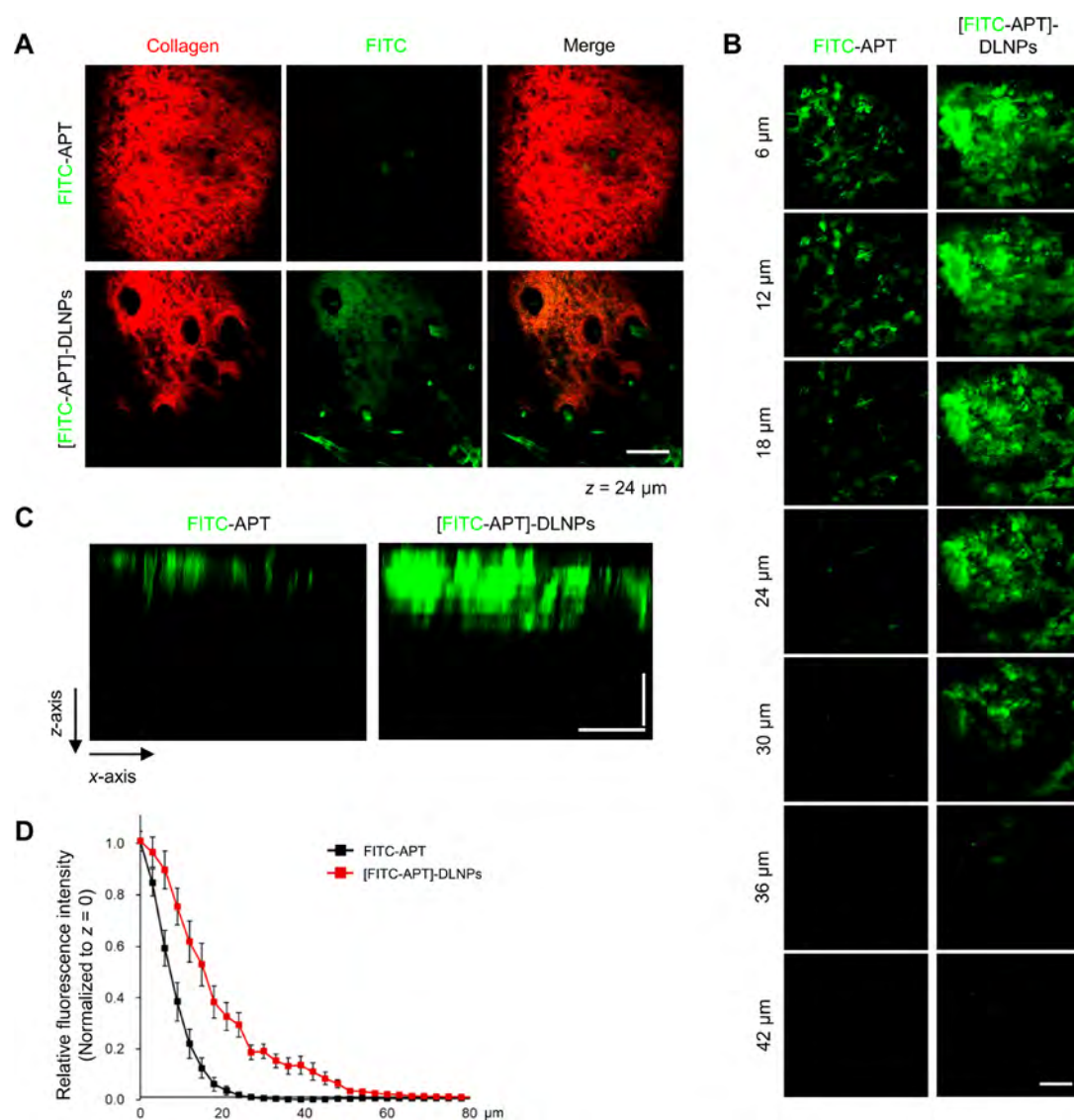


**Figure 5.** Transcutaneously administered aptide-encased DLNPs penetrate into the skin. FITC-APT ( $20 \mu\text{g}$ ) or [FITC-APT]-DLNPs ( $20 \mu\text{g}$  aptide) was transcutaneously applied to the inside ear skin of a disease-free and imiquimod-induced psoriasis mouse. Skin specimens were mounted between glass slides for imaging 6 h after the application of each preparation. Images were acquired using a two-photon microscope. (A) Representative images from a disease-free mouse. Optical sections of the upper dermis at a depth of  $24 \mu\text{m}$  below the skin surface revealed SHG signals of collagen fibers. Scale bar,  $100 \mu\text{m}$ . (B) Representative serial images from a psoriasis model mouse showing psoriasis-like ear skin at intervals of  $6 \mu\text{m}$  below the skin surface. Scale bar,  $100 \mu\text{m}$ . (C) Representative  $x$ - $z$  axis orthogonal images of psoriasis-like ear skin. Horizontal scale bar,  $100 \mu\text{m}$ ; vertical scale bar,  $25 \mu\text{m}$ . (D) Quantitative analysis of relative fluorescence signals in psoriasis-like ear skin. Average signals were plotted as a function of depth by collecting fluorescence signals for each specimen, subtracting values for untreated specimens from each treated specimen, and normalizing to the signal at  $z = 0 \mu\text{m}$ . Data are presented as means  $\pm$  SEM ( $n = 4$  mice/group). FITC-APT, FITC-labeled APTstat3-9R.

mouse ear, an aqueous solution of APTstat3-9R ( $100 \mu\text{g}$  in total; twice a day) caused no appreciable amelioration of psoriasis-like skin inflammation (Figure S4), suggesting extremely low permeability of the pristine APTstat3-9R across the skin. This observation contrasts with the efficacy of intradermally injected peptide (see Figure 2). To overcome this formidable barrier, we developed a transdermal delivery formulation for APTstat3-9R based on complexation with specific lipids. Among known lipid-based formulations, we paid particular attention to specific phospholipids used for formation of bicelles (bilayer + micelle), which have a discoidal nanostructure, because such nanoparticles are shown to enhance transdermal delivery.<sup>31</sup> One specific bicelle formulation, consisting of the long-chain phospholipid, 1,2-

dimyristoyl-*sn*-glycero-3-phosphocholine (DMPC) and short-chain phospholipid, 1,2-dihexanoyl-*sn*-glycero-3-phosphocholine (DHPC), has been shown to self-assemble to form discoidal nanostructures.<sup>31–33</sup> With this precedent-setting study in mind, we used a film formation-rehydration method to first examine whether these two phospholipids are capable of self-assembling into nanostructures containing APTstat3-9R (Figure S5 and Figure 4). By varying the molar ratio of DMPC to DHPC, we constructed various lipid nanocomplexes without and with APTstat3-9R (10 wt %) and characterized their morphology using transmission electron microscopy (TEM). As the DMPC/DHPC molar ratio increased from 1:1 to 2:1 to 3:1, the morphology of the lipid nanoparticles changed from spherical to discoidal in shape (Figure S6).

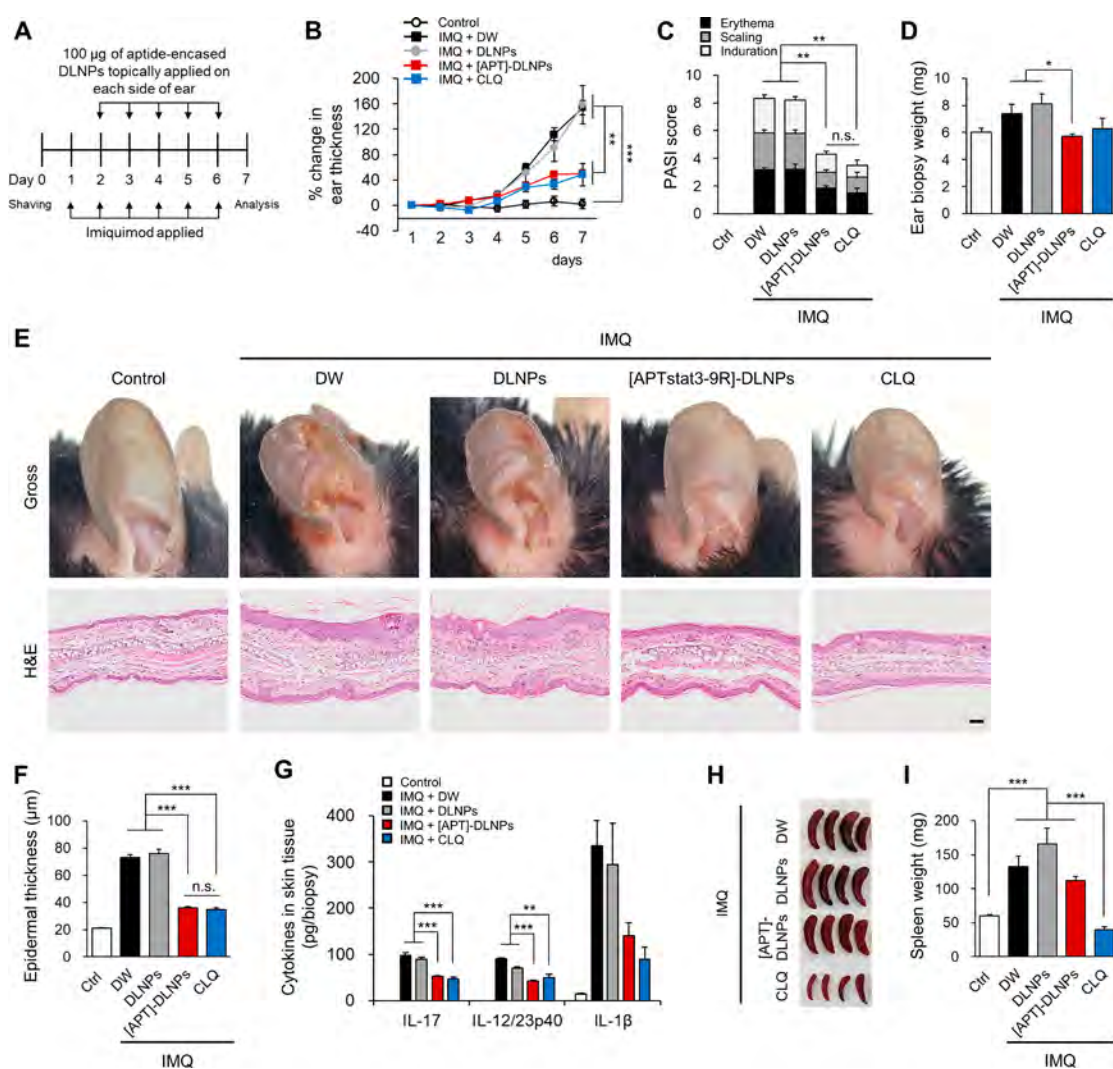


**Figure 6.** Transcutaneous administration of [APTstat3-9R]-DLNPs ameliorates local psoriasis-like skin inflammation. (A) Experimental protocol. Over the course of imiquimod-induced psoriasis-like ear skin inflammation, an equivalent volume of distilled water (DW), DLNPs (0.5 mg), [APT]-DLNPs (50  $\mu$ g aptide), or CLQ (20 mg/cm<sup>2</sup>) was applied transcutaneously twice per day at a 4 h-interval beginning on day 2 of imiquimod application and continuing to day 6. (B) Ear thickness during the course of treatment. Ear thickness is expressed as a percentage of that in disease-free controls. (C) Clinical score of skin erythema, scaling, and induration at day 7. Each score is summed and expressed as a cumulative score. In (B) and (C), clinical parameters were assessed as described in **Materials and Methods**. (D) Ear skin punch biopsy weights. (E) Representative phenotypic presentation (top) and histological images of H&E staining (bottom) of mouse ear skin after 6 days of transcutaneous application of DW, DLNPs, [APT]-DLNPs, or CLQ. Scale bar, 100  $\mu$ m. (F) Quantification of epidermal thickness. (G) Levels of inflammatory cytokines in ear skin homogenates. (H) Representative gross image of spleens at day 7. (I) Spleen weights at day 7. Data are presented as means  $\pm$  SEM ( $n = 6-7$  mice/group; \* $P < 0.05$ , \*\* $P < 0.01$ , and \*\*\* $P < 0.001$ ; one-way ANOVA with *post hoc* Tukey test). Ctrl, Vaseline-applied mice; IMQ, imiquimod-applied mice; APT, APTstat3-9R; CLQ, clobetasol propionate cream.

Notably, at a molar ratio of 3:1, the incorporation of APTstat3-9R (10 wt %) dramatically increased the number of DLNPs compared with that observed in the absence of the aptide (Figure S6 and Figure 4b). TEM images revealed a mean size of these DLNPs in a dry state of  $31.3 \pm 6.8$  nm, with thickness of  $7.7 \pm 1.4$  nm (Figure 4C). Dynamic light scattering (DLS) measurements further showed that a 3:1 molar ratio of the two lipids resulted in formation of the smallest APTstat3-9R-containing nanoparticles ( $\sim 20-30$  nm) (Figure S7A,B). In addition,  $\zeta$  potential measurements showed that, unlike bare lipid nanoparticles, DLNPs formed in the presence of APTstat3-9R exhibited a positive surface charge (Figure S7C), suggesting successful loading of the aptide into the nanoparticles. Notably, there was a drastic difference in colloidal stability between DLNPs with and without APT-

stat3-9R: Whereas bare DLNPs without APTstat3-9R aggregated within 1 h at ambient temperature, APTstat3-9R-encased DLNPs retained their original size for more than 15 days (Figure 4D, E). As the guanidine side chain of arginine can form hydrogen bonds with the phosphate anion of DNA or RNA,<sup>34</sup> we speculate that the arginine residues in the APTstat3-9R may interact with the phosphate anion in DMPC/DHPC lipids, forming the more stable DLNPs than the corresponding nanoparticles without the peptide. For nanoparticles with the same formulation, a smaller size could result in more efficient skin penetration. Accordingly, we selected the smallest-sized, discoid-shaped nanoparticles (*i.e.*, those with a molar ratio of 3:1 DMPC/DHPC), designated [APTstat3-9R]-DLNPs, for subsequent experiments. The stability of [APTstat3-9R]-DLNPs was further assessed in

distilled water (DW), PBS, and 5% fetal bovine serum (FBS) containing DW by DLS. FBS contains similar lipid components as found in the skin layers, including free fatty acids, cholesterol, triglycerides, and phospholipids.<sup>35,36</sup> The nanoparticles, unlike incubation in DW and PBS, became disrupted rapidly in 5% FBS containing DW (Figure S8), suggesting that [APTstat3-9R]-DLNPs would become disintegrated during skin penetration and release the free APTstat3-9R.

**Skin-Penetrating Ability of [APTstat3-9R]-DLNPs.** We next examined whether [APTstat3-9R]-DLNPs are able to penetrate the SC layer after transcutaneous application. In this experiment, FITC-labeled APTstat3-9R was employed to allow tracking/visualization of penetration by monitoring fluorescence. [FITC-APTstat3-9R]-DLNP or FITC-APTstat3-9R alone was topically applied on the shaved skin of a disease-free or psoriatic mouse ear. Two-photon microscopy was employed to visualize and quantify the efficiency of transcutaneous delivery of [FITC-APTstat3-9R]-DLNPs. Image analysis of the untreated skin was also conducted as a technical control to avoid autofluorescence-based false-positive results. Normal mouse ear skin treated with [FITC-APTstat3-9R]-DLNPs exhibited a greater fluorescence signal in deeper layers of the skin compared with skin treated with FITC-APTstat3-9R alone (Figure S9). Fluorescence signal was clearly observed along the boundary of typical hexagonal structure of corneocytes that are terminally differentiated keratinocytes, suggesting paracellular penetration of [APTstat3-9R]-DLNPs through the intercorneocytes gaps. In particular, second-harmonic generation (SHG) signals of collagen in tissue sections at a depth of approximately 24  $\mu\text{m}$  from the top appeared as red fiber structures, indicative of the dermal layer.<sup>37,38</sup> Treatment with [FITC-APTstat3-9R]-DLNPs yielded an appreciable fluorescence signal at the upper dermis, whereas FITC-APTstat3-9R alone seemed to permeate up to the SC layer (Figure 5A). We then assessed skin-penetrating capability using the psoriatic mouse ear skin, in which the polarity of cells is impaired as a consequence of abnormal proliferation of keratinocytes. As shown in Figure 5B,C, a clear fluorescence signal, distributed at depths from  $\sim 40$  to  $60 \mu\text{m}$  from the skin surface, was observed in skin treated with [FITC-APTstat3-9R]-DLNPs; treatment with the aptide alone resulted in penetration up to depth of  $\sim 10$ – $20 \mu\text{m}$ . To quantify the penetration depth into the skin, we analyzed  $x$ – $y$  plane fluorescence signals as a function of the  $z$ -axis depth. All fluorescence signals acquired from the area of interest in each skin specimen were normalized to the signal of untreated control skin specimens at a depth of  $z = 0 \mu\text{m}$ . A quantitative analysis revealed that, following application to normal skin, both [FITC-APTstat3-9R]-DLNPs and the aptide alone showed a similar pattern, characterized by an exponential decrease in epidermal layer fluorescence signals to a depth of  $\sim 20 \mu\text{m}$ ; however, the fluorescence signal intensity of [FITC-APTstat3-9R]-DLNPs trended higher from the epidermis to the upper dermis layer compared with aptide alone (Figure S9C). Notably, there was a clearer difference in penetration ability between the two groups in psoriatic ear skin; the fluorescence signal intensity of [FITC-APTstat3-9R]-DLNPs was always significantly higher than that of the aptide alone in all layers of the skin, from the surface and SC to the dermis layer at a depth greater than  $\sim 60 \mu\text{m}$  (Figure 5D). Collectively, these findings indicate that DLNPs have potential

for use as an efficient transcutaneous delivery formulation for aptides.

**Topical Treatment with [APTstat3-9R]-DLNPs Effectively Ameliorates Psoriasis-like Skin Inflammation.** The efficacy of [APTstat3-9R]-DLNPs against psoriasis-like skin inflammation was evaluated by directly spreading a [APTstat3-9R]-DLNP solution on the ears of imiquimod-induced psoriatic model mice twice per day with 8 h interval (Figure 6A). Compared with distilled water and DLNP vehicle controls, [APTstat3-9R]-DLNPs significantly reduced manifestations of disease over time, including ear thickness, PASI scores, and ear edema (Figure 6B–D). Consistent with these assessment results, gross findings were also improved in [APTstat3-9R]-DLNP-treated skin. Histological analyses showed marked epidermal hyperplasia and infiltration of inflammatory cells in control mice treated with distilled water or DLNP vehicle alone, whereas [APTstat3-9R]-DLNP-treated skin exhibited a clear reduction in these pathological findings (Figure 6E,F). In addition, production of the psoriasis-related cytokines, IL-17, IL-12/23p40 and IL-1 $\beta$ , by the affected skin was significantly reduced by [APTstat3-9R]-DLNPs (Figure 6G). Clobetasol propionate (CLQ), a corticosteroid used to treat psoriasis in the clinic, also ameliorated the aforementioned symptoms to an extent similar that produced by [APTstat3-9R]-DLNPs. As expected, the size and weight of the spleen increased in imiquimod-treated mice, except in the CLQ-treated group, where the spleen appeared to have atrophied, indicative of adverse systemic effects of the corticosteroid drug (Figure 6H,I). Taken together, these results suggest that transcutaneous delivery of [APTstat3-9R]-DLNPs effectively ameliorates psoriasis-like skin inflammation and, unlike conventional corticosteroid drugs, does so without affecting systemically.

In the current study, we described the biological activity and therapeutic efficacy of the STAT3-inhibiting peptide, APTstat3-9R, against psoriasis-like skin inflammation and report the development of a transcutaneous delivery system for peptide therapeutics based on a discoidal lipid nanoparticle formulation. We showed that APTstat3-9R suppressed psoriasis-related cytokine signaling in effector cells through inhibition of STAT3 phosphorylation. Moreover, complexation of APTstat3-9R with specific lipids at a certain ratio resulted in formation of discoidal nanoparticles of  $\sim 20$ – $30 \text{ nm}$  in diameter and enabled transcutaneous delivery of the peptide into epidermal and dermal layers. Finally, we demonstrated that these peptide-encased discoidal nanoparticles effectively treated psoriasis-like skin inflammation.

A number of reports have described the successful transdermal delivery of macromolecules using skin-penetrating peptides, including Poly-R, SPACE, TD-1, DLP and LP-12, consisting of short amino acid sequences.<sup>34,39–42</sup> Based on these findings, we initially expected that our 9R-tagged aptide, APTstat3-9R, would also be able to penetrate the SC layer. However, unlike previously reported cases, APTstat3-9R showed little penetration, as confirmed by two-photon microscopic analysis and *in vivo* efficacy tests. Thus, we devised a transdermal delivery system using two phospholipids, DMPC and DHPC, that have been utilized to prepare bicelles (discoidal lipid nanoparticles).<sup>31</sup> Surprisingly, our aptide-encased or -complexed bicelles exhibited dramatically enhanced colloidal stability in aqueous medium compared with similar bicelles comprising only the two lipids. Due to the presence of arginine in the APTstat3-9R, it is possible to

interact with phospholipids and make relatively more stable nanoparticles. We speculated that similarities in the composition of lipids in nanoparticles with those in the skin layers would facilitate transdermal delivery of bicelles. These lipids can attach themselves to the skin surface, promote adhesiveness, and protect against water loss from the skin; they also gradually lead to loosening of the lipid structure and even cause lipid exchange between intercellular lipid domains.<sup>24,25,43</sup> Moreover, the ultrasmall size of the lipid nanoparticles (~20 nm) would facilitate penetration through the narrow intercellular spaces or gaps in the SC layer. Indeed, APTstat3-9R-encased discoidal nanoparticles (APTstat3-9R)-DLNPs) applied to the skin successfully passed through the SC layer and reached both epidermal and dermal layers in psoriasis-like mouse skin. Therefore, the ultrasmall lipid nanoparticle formulation is a key factor enabling transdermal delivery and therapeutic efficacy of the peptide inhibitor. Although there are differences between mouse and human models, including skin thickness, results of two-photon microscopy-based skin penetration and therapeutic efficacy tests in a psoriasis-like inflammation model clearly show the potential of these discoidal lipid nanoparticles as a transcutaneous delivery system.

The first clinically relevant aspect of our study relates to our assessment of a STAT3-inhibiting peptide in an inflammatory skin disease. Most treatments for chronic inflammatory skin disease are accompanied by broad immunosuppression. Because the immunopathogenesis of psoriasis is generally understood, regulation of cytokine signaling is considered an ideal strategy for developing drugs intended to modulate inflammation. Recently, biologic agents targeting the psoriasis-related cytokines IL-12/23p40 (ustekinumab) and IL-17 (ixekizumab and secukinumab) have been developed.<sup>44–46</sup> In addition to biologics that target extracellular cytokines, JAK inhibitors such as tofacitinib have been developed, premised on the idea that inflammatory cytokines that act primarily through the JAK-STAT pathway are involved in inducing inflammation and impaired barrier function.<sup>47,48</sup> However, those biologics and JAK inhibitors carry a risk of unexpected adverse systemic events, such as sepsis, opportunistic infections, and pulmonary tuberculosis. Consequently, a highly efficient inhibitor that targets STAT3 directly, such as the APTstat3-9R peptide described here, represents a notable development as it does not exert unintended consequences on other signaling pathways and thus may have minimal adverse effects.

The second clinically relevant aspect of our study is the development of a technically feasible transcutaneous delivery system for peptide therapeutics, formed by simply complexing peptide with biocompatible lipids. The resulting peptide-encased DLNPs were not only able to partly overcome the formidable physical barrier posed by the skin, but would also satisfy safety requirements for delivery formulations and criteria for patient compliance. Topical therapies are the mainstay of therapeutic options for the majority of patients with psoriasis, either as monotherapy or in combination with phototherapy, systemic therapy, and/or biologic therapy. Thus, the lipid formulation-based transcutaneous delivery system demonstrated here could be applicable to treatment of other skin inflammation diseases, including atopic dermatitis.

Lastly, the STAT3-inhibiting peptide has potential for use in treating many other diseases, ranging from cancer to inflammation-associated diseases,<sup>6,7</sup> in which aberrant activa-

tion of STAT3 is a critical feature. For example, it has been shown that STAT3 plays a key role in the pathogenesis of pulmonary fibrosis, kidney fibrosis, and nonalcoholic steatohepatitis. Thus, the [APTstat3-9R]-DLNPs developed here could be used against these hard-to-treat diseases.

## CONCLUSION

In summary, we demonstrated that [APTstat3-9R]-DLNPs efficiently penetrate the skin and exert an anti-inflammatory effect in a preclinical model of psoriasis through modulation of cytokine signaling. DLNP-assisted transcutaneous delivery of a STAT3-inhibiting peptide could be a promising strategy for treating psoriatic skin inflammation without causing adverse systemic events. Furthermore, the DLNP system could be applied to the transdermal delivery of other bioactive peptide candidates.

## MATERIALS AND METHODS

All aptides, including APTstat3-9R, FITC-labeled APTstat3-9R and APTscr-9R, were custom synthesized by AnyGen (Gwangju, Korea). All phospholipids, including DMPC and DHPC, were purchased from Avanti Polar Lipids (Alabaster, AL, USA).

**Cell Lines and Culture.** HaCaT (human keratinocytes), NIH3T3 (mouse embryonic fibroblasts), and A549 (human lung adenocarcinoma) cell lines were obtained from the American Type Culture Collection (ATCC; Manassas, VA, USA) and were cultured in Dulbecco's modified Eagle medium (DMEM; Gibco, Grand Island, NY, USA) supplemented with 10% fetal bovine serum (FBS; Gibco) and 1% penicillin/streptomycin under a humidified atmosphere containing 5% CO<sub>2</sub> at 37 °C.

**Mice.** C57BL/6 wild-type female mice (6–8 weeks old) were purchased from Orient Bio Inc. (Seongnam, Korea) and maintained under pathogen-free conditions in the animal facility for at least 1 week. All animal studies were performed in accordance with the NIH Guide for the Care and Use of Laboratory Animals (National Academies Press, 2011). All animal experimental protocols were approved by the Institutional Animal Care and Use Committee of the Korea Advanced Institute of Science and Technology (KAIST).

**Preparation and Characterization of Aptide-Encased DLNPs.** [APTstat3-9R]-DLNPs were prepared using a thin-film hydration method. Discotic phospholipid nanoparticles were formed using DMPC as the long-chain phospholipid and DHPC as the short-chain phospholipid, as described previously.<sup>31,32</sup> Briefly, DMPC and DHPC were dissolved in chloroform and mixed at the appropriate ratios. The lipid mixture was then vortexed and evaporated under a stream of nitrogen gas to yield a thin lipid film. The lipid film was subsequently hydrated with distilled water to a concentration of 1 w/v % of total lipid and sonicated at room temperature until a transparent solution was acquired. [APTstat3-9R]-DLNPs were obtained using the same procedure, except that the lipid film was hydrated with an aqueous solution of APTstat3-9R, added at a concentration of 10 wt %.

The size and  $\zeta$  potential of DMPC/DHPC lipid nanoparticles in the absence and presence of APTstat3-9R were determined by dynamic light scattering analysis using a Nanosizer ZS90 (Malvern Instruments, Ltd., Malvern, UK). Nanoparticle morphology was examined by TEM using a JEM-3011 system (JEOL Ltd., Tokyo, Japan) operating at 300 kV. The average diameter of [APTstat3-9R]-DLNPs was determined by analyzing at least 200 nanoparticles using ImageJ software, version 1.49 (National Institutes of Health, Bethesda, MD, USA).

**Generation of BMDCs and BMDMs.** Bone marrow was extracted from femurs and tibias of a mouse by flushing each shaft with RPMI-1640 culture medium (Gibco) using a syringe, after which red blood cells (RBCs) were lysed with RBC lysis buffer (BioLegend, CA, USA). Bone marrow cells were suspended, filtered through a 70  $\mu$ m cell strainer, and resuspended in complete RPMI culture medium containing 10 ng/mL of granulocyte-macrophage colony-stimulating

factor (GM-CSF; CreaGene, Seongnam, Korea) and IL-4 (CreaGene). Cells were seeded in 24-well plates at  $1 \times 10^6$  cells/well. The medium was replaced every 2 days, and nonadherent and loosely adherent cells were collected and replated after 6 days. Differentiation of BMDMs was induced by culturing bone marrow cells in complete DMEM medium containing 10 ng/mL of macrophage colony-stimulating factor (M-CSF; CreaGene).

For experiments in which BMDCs and BMDMs were stimulated with a TLR7 ligand, cells were first treated with phosphate-buffered saline (PBS), APTscr-9R (20  $\mu$ M), or APTstat3-9R (1, 5, 10, or 20  $\mu$ M) for 6 h and then cultured in the presence of 1  $\mu$ g/mL R848 (resiquimod; Sigma-Aldrich, St. Louis, MO, USA) for 18 h. After 24 h, supernatants were collected for determination of IL-1 $\beta$  and IL-12/23 p40 levels, measured by enzyme-linked immunosorbent assay (ELISA).

**Isolation, Culture, and Stimulation of  $\gamma\delta$ -T Cells.** Mouse  $\gamma\delta$ -T cells were freshly isolated from spleen and lymph nodes using a TCR $\gamma\delta^+$  T cell isolation kit (Miltenyi Biotec, Auburn, CA, USA) according to the manufacturer's protocol. The purity of isolated  $\gamma\delta$ -T cells was >85%. Isolated  $\gamma\delta$ -T cells were pretreated with PBS, APTscr-9R (10  $\mu$ M), or APTstat3-9R (10  $\mu$ M) for 4 h and then stimulated with recombinant IL-1 $\beta$  (10 ng/mL; PeproTech, Rocky Hill, NJ, USA) and recombinant IL-23 (50 ng/mL; eBioscience, San Diego, CA, USA), without anti-CD3e antibody, for 12 h. Supernatants were harvested for measurement of IL-17A by ELISA.

**In Vitro Cell Uptake Assay.** Cellular uptake of aptide was determined by flow cytometry and confocal microscope using FITC-labeled APTstat3-9R. HaCaT and NIH3T3 cells were treated with different concentrations (1, 5, or 10  $\mu$ M) of FITC-labeled APTstat3-9R for varying durations (0.25, 0.5, 1, 2, 4, or 8 h). The cells were washed twice with PBS to remove peptides that were not taken up, after which intracellular fluorescence intensity was analyzed by flow cytometry (LSR II; BD Bioscience, San Jose, CA, USA) using FlowJo software (Tree Star Inc., San Carlos, CA, USA). Intracellular localization was confirmed by seeding HaCaT and NIH3T3 cells on sterilized coverslips and treating with FITC-labeled APTstat3-9R at a concentration of 10  $\mu$ M for 6 h. The cells were washed, fixed with 4% paraformaldehyde (PFA), and then mounted in Vectashield mounting medium containing 4',6-diamidino-2-phenylindole (DAPI; Vector Laboratories, Burlingame, CA, USA) to allow visualization of nuclei. Intracellular fluorescence intensity and localization were analyzed using a LSM 780 confocal microscope (Carl Zeiss, Oberkochen, Germany) with ZEN software (Carl Zeiss).

**Cell Viability Assay.** Cell viability was evaluated using a WST-1 assay (Roche, Indianapolis, IN, USA) according to the manufacturer's instructions. HaCaT, NIH3T3, and A549 cells and isolated BMDCs were seeded in a 96-well plate and incubated overnight. Cells were treated with PBS, APTscr-9R, or different concentrations of APTstat3-9R for 12 or 24 h, after which WST-1 reagent (10  $\mu$ L) was added, and plates were incubated for an additional 2 h. Absorbance was measured at 440 nm using a microplate reader (VersaMax; Molecular Devices, Sunnyvale, CA, USA). Viability of aptide-treated cells was expressed relative to that of control cells as a percentage.

**Determination of Cytokine Release and STAT3 Inhibition *in Vitro*.** Concentrations of IL-17A, IL-12/23 p40, and IL-1 $\beta$  in culture supernatants were measured using DuoSet ELISA kits (R&D Systems, Minneapolis, MN, USA), according to the manufacturer's protocols. STAT3 inhibition *in vitro* was determined by Western blot analysis and intracellular phospho-protein staining assay. Before activating STAT3 by stimulating with IL-6, HaCaT cells were cultured in serum-free medium for at least 12 h and then pretreated with PBS, APTscr-9R (10  $\mu$ M), or APTstat3-9R (10  $\mu$ M) for 1 h. Cells were further stimulated with recombinant IL-6 (25 ng/mL; R&D Systems) for 30 min. HaCaT cells were lysed using a Protein Extraction kit (Pro-Prep; Intron Biotechnology, Seongnam, Korea). Total protein concentration was measured using a Bradford assay. Equal amounts of proteins were separated by sodium dodecyl sulfate-polyacrylamide gel electrophoresis (SDS-PAGE) on a 10% gel and transferred to a polyvinylidene difluoride (PVDF) membrane. The membrane was

blocked in 5% bovine serum albumin (BSA) in Tris-buffered saline containing Tween-20 (TBST) at room temperature for 1 h and incubated with the following primary antibodies: antiphospho-STAT3 (Tyr705) (Cell Signaling, Beverly, MA, USA), anti-STAT3 (Cell Signaling), and anti-GAPDH (Abcam, Cambridge, UK). The membrane was then incubated with horseradish peroxidase (HRP)-conjugated secondary antibody, and immunoreactive proteins were visualized using an enhanced chemiluminescence (ECL) detection kit (GE Healthcare, Little Chalfont, UK).

Phosphorylation of STAT3 was determined in splenic mononuclear cells by flow cytometry using BD Phosflow reagents (BD Bioscience) according to manufacturer's instructions. Briefly, splenic mononuclear cells were isolated by mincing the tissue through a 70- $\mu$ m cell strainer. The cells were first treated with PBS, APTscr-9R (10  $\mu$ M), or APTstat3-9R (10  $\mu$ M) for 1 h and then stimulated *in vitro* with recombinant IL-1 $\beta$  (10 ng/mL) and IL-23 (50 ng/mL) without anti-CD3e antibody for 30 min. After washing, cells were permeabilized with prechilled pure methanol and then stained with phycoerythrin (PE)-conjugated mouse anti-STAT3 (pY705) monoclonal antibody (BD Bioscience). Stained cells were analyzed by flow cytometry.

**Two-Photon Microscopy.** Our two-photon microscopy system was built on a previously described video-rate laser-scanning two-photon microscope platform.<sup>49</sup> The system uses a mode-locked tunable Ti:sapphire laser with a wavelength range from 690 to 1020 nm (Chameleon Ultra; Coherent) for two-photon excitation. A prism pair (10SF10; Newport) was adapted to the system for dispersion compensation. For video-rate raster scanning, the system has a custom-developed scanner consisting of a gold-coated polygonal mirror (BMC-7; Lincoln Laser) and a galvanometer (6240H; Cambridge Technology, Bedford, MA, USA). The two-dimensional (2D) field of view is approximately 400  $\times$  400  $\mu$ m when a 25 $\times$  objective lens (CFI75 Apo LWD 25XW, NA1.1, Nikon) is used. Fluorescence signals with three different bands (CFP/SHG, GFP, RRP) can be simultaneously detected using three bandpass filters (FF01-420/5, FF01-525/45, FF01-585/40; Semrock, Rochester, NY, USA) and three photomultiplier tubes (R7518; Hamamatsu). 2D images (512  $\times$  512 pixels) are stored on a hard disk at a frame rate of 30 Hz using custom-written software and Matrox Imaging Library (MIL9).

**In Vivo Transcutaneous Delivery.** Damage to the outermost layer of the skin was minimized by carefully performing transcutaneous application, avoiding procedures that involve SC manipulation, such as tape-stripping and brushing methods. Hair was gently removed from both ears of the mouse using a depilatory cream under anesthesia with a 30 mg/kg tiletamine/zolazepam solution containing 10 mg/kg of xylazine. The ear skin was cleaned with distilled water and wiped with a cotton swab. Transcutaneous delivery of APTstat3-9R was visualized by gently applying FITC-APT (20  $\mu$ g) or [FITC-APT]-DLNPs (20  $\mu$ g aptide) to the inside ear skin of a disease-free mouse or imiquimod-induced psoriasis mouse. After 6 h, the application site was cleaned with a cotton swab, and the ear skin was harvested and mounted between glass slides for two-photon imaging. For two-photon microscopy, samples were excited at 840 nm with a femto-second Ti:sapphire laser at a beam power of 30 mW using a 25 $\times$  water-immersion objective lens (CFI75 Apo LWD 25XW). SHG and green fluorescence signals were collected through bandpass filters (FF01-420/5, FF01-525/45; Semrock) separated by a dichroic mirror (FF495/Di03, FF555/Di02; Semrock). Images were captured at sequential 3  $\mu$ m intervals from the skin surface. Intensity profiles of FITC signal *versus* depth of the skin were plotted by determining the average pixel intensity of four randomly defined regions using the 'plot z-axis profile' plugin in ImageJ software.<sup>50</sup> The surface of the skin (0  $\mu$ m depth) was defined as the point of maximum FITC signal. Untreated skin specimens were also imaged to eliminate signals attributable to autofluorescence of the skin. The  $x$ - $z$  axis sectioned orthogonal view of the skin was reconstructed using the "volume viewer" plugin in ImageJ software.

**Imiquimod-Induced Psoriasis Mouse Model and *in Vivo* Treatment.** For the imiquimod-induced psoriasis model, mice received a daily topical dose of 62.5 mg of imiquimod 5% cream

(Aldara; 3 M Pharmaceuticals, Leicestershire, UK) on the shaved skin of their back and each ear for 6 consecutive days. An equivalent amount of petroleum jelly (Vaseline; Unilever, London, UK) was topically applied to mice in the disease-free control group. Two hours after imiquimod cream application, mice in the control group received an intradermal injection of APTscr-9R (50  $\mu\text{g}$ ), APTstat3-9R (50  $\mu\text{g}$ ), or an equal volume of PBS (20  $\mu\text{L}$ ) in the delimited area of the back skin using a 30 gauge needle twice a day for 6 days. All therapeutics were applied under anesthesia with 30 mg/kg of tiletamine/zolazepam and 10 mg/kg of xylazine. On day 7, mice were sacrificed, and full-thickness skin samples of identical areas were obtained using 5 mm punch biopsy tools. The spleen was also removed and weighed.

Alternatively, in experiments designed to evaluate the efficacy of topically applied APTstat3-9R, a daily dose of 20 mg/cm<sup>2</sup> of imiquimod 5% cream was topically applied to the inside of each ear for 6 consecutive days.<sup>51</sup> Mice were randomly divided into five groups. From days 2 to 6, DLNPs (0.5 mg), [APTstat3-9R]-DLNPs (50  $\mu\text{g}$ , 10 wt %), clobetasol propionate cream (20 mg/cm<sup>2</sup>, Dermovate cream; GSK, Brentford, UK), or an equal volume of distilled water (25  $\mu\text{L}$ ) was topically applied to the inside of each ear 4 h before and after imiquimod application so as to minimize interactions between the two preparations. The disease-free control group was as described above.

A clinical assessment of the severity of psoriatic skin lesions was performed daily using Psoriasis Area and Severity Index (PASI) scores, which rates erythema, scaling, and thickness on a scale of 0 to 4, as follows: 0, no symptoms; 1, mild; 2, moderate; 3, severe; and 4, very severe. Ear thickness and back skinfold thickness were measured daily in triplicate using a micrometer (Mitutoyo, Kawasaki, Japan) before treatment. The percentage change from baseline was calculated.

**Preparation of Skin Tissue for Histological Analysis.** Skin samples were fixed in 4% PFA, embedded in paraffin, and sectioned at 5  $\mu\text{m}$  thickness. Tissue sections were stained with hematoxylin and eosin using a standard protocol and then analyzed on an Eclipse Ni-E upright microscope (Nikon Corporation, Tokyo, Japan). Epidermal thickness was measured based on at least 50 hand-drawn line segments connecting the SC to the dermal-epidermal junction (DEJ) for each section using NIS-elements microscopic imaging software (Nikon).

For immunohistochemistry, skin sections were deparaffinized in xylene and rehydrated in distilled water. Antigen retrieval was performed by immersing slides in boiling sodium citrate buffer (10 mM sodium citrate, pH 6.0) for 10 min, after which slides were placed in 1% sodium hydroxide and 1% hydrogen peroxide in distilled water for 20 min to quench endogenous peroxidase activity. Nonspecific binding was blocked by incubating sections with Tris buffer containing 3% BSA and 0.2% Triton X-100 for 1 h at room temperature, after which sections were incubated with antiphospho-STAT3 (Tyr705) antibody (1:100; Cell Signaling) or anti-IL-17 antibody (1:100; Abcam) for 24 h at 4 °C. Slides were then washed and incubated with biotinylated goat antirabbit secondary antibody (1:200; Vector Laboratories) for 1 h at room temperature. All slides were rinsed and incubated with Vectastain Elite ABC kit (Vector Laboratories) for 30 min followed by incubation with DAB substrate (Vector Laboratories) for 5 min. Finally, slides were counterstained with hematoxylin and examined under a microscope. Phosphorylated STAT3-positive areas were expressed as a percentage of the total area of the image. Areas in five random sections per mouse were quantified using ImageJ software.

**Measurement of Inflammatory Cytokines in Skin Homogenates.** Total protein from skin samples was extracted by adding tissue protein extraction reagent (T-PER; Thermo Scientific, Waltham, MA, USA) supplemented with protease inhibitor cocktail (Thermo Scientific). The samples were homogenized using a disposable micro homogenizer (Biomasher II; Takara Bio Inc., Shiga, Japan) and then centrifuged to remove debris. Aliquots of the supernatant were used for the assay. The concentrations of IL-17A, IL-12/23 p40, and IL-1 $\beta$  in supernatants were measured using ELISA kits (R&D Systems), as indicated above.

**Statistical Analysis.** Data are expressed as means  $\pm$  SEM unless otherwise noted. Differences among groups were analyzed by one-way analysis of variance (ANOVA) followed by *post hoc* Tukey test. All statistical analyses were performed using SPSS Statistics 20 software (SPSS Inc.), and *P* values <0.05 were considered statistically significant.

## ASSOCIATED CONTENT

### Supporting Information

The Supporting Information is available free of charge on the ACS Publications website at DOI: 10.1021/acsnano.8b02330.

Viability of NIH3T3 cells following exposure to APTstat3-9R (Figure S1), Topical imiquimod causes adverse systemic effects (Figure S2), IL-17 expression in imiquimod-induced psoriatic skin lesions (Figure S3), Transcutaneous administration of APTstat3-9R to imiquimod-induced psoriasis-like ear skin (Figure S4), Graphic representation of the scheme for preparing aptide-encased discoid-shaped lipid nanoparticles (Figure S5), TEM images of lipid nanoparticles at different DMPC/DHPC molar ratios in the absence or presence of APTstat3-9R (Figure S6), Analysis of hydrodynamic size and zeta potential (Figure S7), The stability of [APTstat3-9R]-DLNPs in various solutions (Figure S8), Optical sectioning by multiphoton microscopy (Figure S9) (PDF)

## AUTHOR INFORMATION

### Corresponding Author

\*E-mail: syjon@kaist.ac.kr.

### ORCID

Jin Yong Kim: 0000-0002-1278-7491

Jinhyo Ahn: 0000-0001-9343-5932

Jinjoo Kim: 0000-0002-2702-6871

Minsuk Choi: 0000-0002-6181-3051

Hyungsu Jeon: 0000-0002-6474-4506

Kibaek Choe: 0000-0002-3068-6088

Dong Yun Lee: 0000-0003-4613-6838

Pilhan Kim: 0000-0001-8388-1840

Sangyong Jon: 0000-0002-6971-586X

### Author Contributions

J.Y.K. and S.J. conceived the idea and designed experiments. J.Y.K. performed most of the experiments, interpreted data, and wrote the manuscript. J.K., M.C., H.J., and D.Y.L. performed some experiments. J.Y.K., J.A., K.C., and P.K. performed two-photon imaging and evaluated the data. S.J. supervised the project and wrote the manuscript.

### Notes

The authors declare no competing financial interest.

## ACKNOWLEDGMENTS

We would like to thank Seo W and Kim J. H. for technical support. This research was supported by a Global Research Laboratory grant (NRF-2012K1A1A2045436) and the Bio & Medical Technology Development Program (NRF-2018M3A9B5023527) through the National Research Foundation of Korea (NRF) funded by the Ministry of Science and ICT.

## REFERENCES

- (1) Nestle, F. O.; Kaplan, D. H.; Barker, J. Psoriasis. *N. Engl. J. Med.* **2009**, *361*, 496–509.
- (2) Michalek, I. M.; Loring, B.; John, S. M. A Systematic Review of Worldwide Epidemiology of Psoriasis. *J. Eur. Acad. Dermatol. Venereol.* **2017**, *31*, 205–212.
- (3) Lowes, M. A.; Suarez-Farinas, M.; Krueger, J. G. Immunology of Psoriasis. *Annu. Rev. Immunol.* **2014**, *32*, 227–255.
- (4) Pasparakis, M.; Haase, I.; Nestle, F. O. Mechanisms Regulating Skin Immunity and Inflammation. *Nat. Rev. Immunol.* **2014**, *14*, 289–301.
- (5) Bromberg, J.; Darnell, J. E., Jr. The Role of STATs in Transcriptional Control and Their Impact on Cellular Function. *Oncogene* **2000**, *19*, 2468–2473.
- (6) Yu, H.; Kortylewski, M.; Pardoll, D. Crosstalk between Cancer and Immune Cells: Role of STAT3 in the Tumour Microenvironment. *Nat. Rev. Immunol.* **2007**, *7*, 41–51.
- (7) Miklossy, G.; Hilliard, T. S.; Turkson, J. Therapeutic Modulators of STAT Signalling for Human Diseases. *Nat. Rev. Drug Discovery* **2013**, *12*, 611–629.
- (8) Sano, S.; Chan, K. S.; Carbajal, S.; Clifford, J.; Peavey, M.; Kiguchi, K.; Itami, S.; Nickoloff, B. J.; DiGiovanni, J. Stat3 Links Activated Keratinocytes and Immuncytes Required for Development of Psoriasis in a Novel Transgenic Mouse Model. *Nat. Med.* **2005**, *11*, 43–49.
- (9) Bettelli, E.; Korn, T.; Oukka, M.; Kuchroo, V. K. Induction and Effector Functions of T(H)17 Cells. *Nature* **2008**, *453*, 1051–1057.
- (10) Chaudhry, A.; Rudra, D.; Treuting, P.; Samstein, R. M.; Liang, Y.; Kas, A.; Rudensky, A. Y. CD4+ Regulatory T Cells Control TH17 Responses in a Stat3-Dependent Manner. *Science* **2009**, *326*, 986–991.
- (11) Di Cesare, A.; Di Meglio, P.; Nestle, F. O. The IL-23/Th17 Axis in the Immunopathogenesis of Psoriasis. *J. Invest. Dermatol.* **2009**, *129*, 1339–1350.
- (12) Mathur, A. N.; Chang, H. C.; Zisoulis, D. G.; Stritesky, G. L.; Yu, Q.; O'Malley, J. T.; Kapur, R.; Levy, D. E.; Kansas, G. S.; Kaplan, M. H. Stat3 and Stat4 Direct Development of IL-17-Secreting Th Cells. *J. Immunol.* **2007**, *178*, 4901–4907.
- (13) Seavey, M. M.; Dobrzanski, P. The Many Faces of Janus Kinase. *Biochem. Pharmacol.* **2012**, *83*, 1136–1145.
- (14) Kim, D.; Lee, I. H.; Kim, S.; Choi, M.; Kim, H.; Ahn, S.; Saw, P. E.; Jeon, H.; Lee, Y.; Jon, S. A Specific STAT3-Binding Peptide Exerts Antiproliferative Effects and Antitumor Activity by Inhibiting STAT3 Phosphorylation and Signaling. *Cancer Res.* **2014**, *74*, 2144–2151.
- (15) Barry, B. W. Breaching the Skin's Barrier to Drugs. *Nat. Biotechnol.* **2004**, *22*, 165–167.
- (16) Alkilani, A. Z.; McCrudden, M. T.; Donnelly, R. F. Transdermal Drug Delivery: Innovative Pharmaceutical Developments Based on Disruption of the Barrier Properties of the Stratum Corneum. *Pharmaceutics* **2015**, *7*, 438–470.
- (17) Prausnitz, M. R.; Langer, R. Transdermal Drug Delivery. *Nat. Biotechnol.* **2008**, *26*, 1261–1268.
- (18) Bos, J. D.; Meinardi, M. M. The 500 Da Rule for the Skin Penetration of Chemical Compounds and Drugs. *Exp. Dermatol.* **2000**, *9*, 165–169.
- (19) Rancan, F.; Gao, Q.; Graf, C.; Troppens, S.; Hadam, S.; Hackbarth, S.; Kembuan, C.; Blume-Peytavi, U.; Ruhl, E.; Lademann, J.; Vogt, A. Skin Penetration and Cellular Uptake of Amorphous Silica Nanoparticles with Variable Size, Surface Functionalization, and Colloidal Stability. *ACS Nano* **2012**, *6*, 6829–6842.
- (20) Prausnitz, M. R.; Mitragotri, S.; Langer, R. Current Status and Future Potential of Transdermal Drug Delivery. *Nat. Rev. Drug Discovery* **2004**, *3*, 115–124.
- (21) Cevc, G. Transfersomes, Liposomes and Other Lipid Suspensions on the Skin: Permeation Enhancement, Vesicle Penetration, and Transdermal Drug Delivery. *Crit. Rev. Ther. Drug Carrier Syst.* **1996**, *13*, 257–388.
- (22) Elsayed, M. M.; Abdallah, O. Y.; Naggar, V. F.; Khalafallah, N. M. Lipid Vesicles for Skin Delivery of Drugs: Reviewing Three Decades of Research. *Int. J. Pharm.* **2007**, *332*, 1–16.
- (23) Muller, R. H.; Radtke, M.; Wissing, S. A. Solid Lipid Nanoparticles (SLN) and Nanostructured Lipid Carriers (NLC) in Cosmetic and Dermatological Preparations. *Adv. Drug Delivery Rev.* **2002**, *54*, S131–S155.
- (24) Zhai, Y.; Zhai, G. Advances in Lipid-Based Colloid Systems as Drug Carrier for Topical Delivery. *J. Controlled Release* **2014**, *193*, 90–99.
- (25) Torchilin, V. P. Recent Advances with Liposomes as Pharmaceutical Carriers. *Nat. Rev. Drug Discovery* **2005**, *4*, 145–160.
- (26) Williams, A. C.; Barry, B. W. Penetration Enhancers. *Adv. Drug Delivery Rev.* **2012**, *64*, 128–137.
- (27) Gao, W.; Vecchio, D.; Li, J.; Zhu, J.; Zhang, Q.; Fu, V.; Li, J.; Thamphiwatana, S.; Lu, D.; Zhang, L. Hydrogel Containing Nanoparticle-Stabilized Liposomes for Topical Antimicrobial Delivery. *ACS Nano* **2014**, *8*, 2900–2907.
- (28) Lee, J.; Chuang, T. H.; Redecke, V.; She, L.; Pitha, P. M.; Carson, D. A.; Raz, E.; Cottam, H. B. Molecular Basis for the Immunostimulatory Activity of Guanine Nucleoside Analogs: Activation of Toll-Like Receptor 7. *Proc. Natl. Acad. Sci. U. S. A.* **2003**, *100*, 6646–6651.
- (29) Kanno, A.; Tanimura, N.; Ishizaki, M.; Ohko, K.; Motoi, Y.; Onji, M.; Fukui, R.; Shimozato, T.; Yamamoto, K.; Shibata, T.; Sano, S.; Sugahara-Tobinai, A.; Takai, T.; Ohto, U.; Shimizu, T.; Saitoh, S.; Miyake, K. Targeting Cell Surface TLR7 for Therapeutic Intervention in Autoimmune Diseases. *Nat. Commun.* **2015**, *6*, 6119.
- (30) Sutton, C. E.; Lalor, S. J.; Sweeney, C. M.; Brereton, C. F.; Lavelle, E. C.; Mills, K. H. Interleukin-1 and IL-23 Induce Innate IL-17 Production from Gammadelta T Cells, Amplifying Th17 Responses and Autoimmunity. *Immunity* **2009**, *31*, 331–341.
- (31) Barbosa-Barros, L.; Rodriguez, G.; Barba, C.; Cocera, M.; Rubio, L.; Estelrich, J.; Lopez-Iglesias, C.; de la Maza, A.; Lopez, O. Bicelles: Lipid Nanostructured Platforms with Potential Dermal Applications. *Small* **2012**, *8*, 807–818.
- (32) Rubio, L.; Alonso, C.; Rodriguez, G.; Barbosa-Barros, L.; Coderch, L.; De la Maza, A.; Parra, J. L.; Lopez, O. Bicellar Systems for *in vitro* Percutaneous Absorption of Diclofenac. *Int. J. Pharm.* **2010**, *386*, 108–113.
- (33) Vestergaard, M.; Kraft, J. F.; Vosegaard, T.; Thogersen, L.; Schiott, B. Bicelles and Other Membrane Mimics: Comparison of Structure, Properties, and Dynamics from MD Simulations. *J. Phys. Chem. B* **2015**, *119*, 15831–15843.
- (34) Koren, E.; Torchilin, V. P. Cell-Penetrating Peptides: Breaking Through to the Other Side. *Trends Mol. Med.* **2012**, *18*, 385–393.
- (35) Pappas, A. Epidermal Surface Lipids. *Derm.-Endocrinol.* **2009**, *1*, 72–76.
- (36) Villard, P. H.; Barlesi, F.; Armand, M.; Dao, T. M.; Pascucci, J. M.; Fouchier, F.; Champion, S.; Dufour, C.; Ginies, C.; Khalil, A.; Amiot, M. J.; Barra, Y.; Seree, E. CYP1A1 Induction in the Colon by Serum: Involvement of the PPARalpha Pathway and Evidence for a New Specific Human PPREalpha Site. *PLoS One* **2011**, *6*, e14629.
- (37) Palero, J. A.; de Bruijn, H. S.; van der Ploeg van den Heuvel, A.; Sterenborg, H. J.; Gerritsen, H. C. Spectrally Resolved Multiphoton Imaging of *In vivo* and Excised Mouse Skin Tissues. *Biophys. J.* **2007**, *93*, 992–1007.
- (38) Li, J. L.; Goh, C. C.; Keeble, J. L.; Qin, J. S.; Roediger, B.; Jain, R.; Wang, Y.; Chew, W. K.; Weninger, W.; Ng, L. G. Intravital Multiphoton Imaging of Immune Responses in the Mouse Ear Skin. *Nat. Protoc.* **2012**, *7*, 221–234.
- (39) Kumar, S.; Zakrewsky, M.; Chen, M.; Menegatti, S.; Muraski, J. A.; Mitragotri, S. Peptides as Skin Penetration Enhancers: Mechanisms of Action. *J. Controlled Release* **2015**, *199*, 168–178.
- (40) Rothbard, J. B.; Garlington, S.; Lin, Q.; Kirschberg, T.; Kreider, E.; McGrane, P. L.; Wender, P. A.; Khavari, P. A. Conjugation of Arginine Oligomers to Cyclosporin A Facilitates Topical Delivery and Inhibition of Inflammation. *Nat. Med.* **2000**, *6*, 1253–1257.

(41) Chen, Y.; Shen, Y.; Guo, X.; Zhang, C.; Yang, W.; Ma, M.; Liu, S.; Zhang, M.; Wen, L. P. Transdermal Protein Delivery by a Coadministered Peptide Identified *via* Phage Display. *Nat. Biotechnol.* **2006**, *24*, 455–460.

(42) Kim, W. J.; Koo, J. H.; Cho, H. J.; Lee, J. U.; Kim, J. Y.; Lee, H. G.; Lee, S.; Kim, J. H.; Oh, M. S.; Suh, M.; Shin, E. C.; Ko, J. Y.; Sohn, M. H.; Choi, J. M. Protein Tyrosine Phosphatase Conjugated with a Novel Transdermal Delivery Peptide, Astrotactin 1-Derived Peptide Recombinant Protein Tyrosine Phosphatase (AP-rPTP), Alleviates Both Atopic Dermatitis-like and Psoriasis-like Dermatitis. *J. Allergy Clin. Immunol.* **2018**, *141*, 137–151.

(43) Bouwstra, J. A.; Honeywell-Nguyen, P. L.; Gooris, G. S.; Ponec, M. Structure of the Skin Barrier and Its Modulation by Vesicular Formulations. *Prog. Lipid Res.* **2003**, *42*, 1–36.

(44) Griffiths, C. E.; Strober, B. E.; van de Kerkhof, P.; Ho, V.; Fidelus-Gort, R.; Yeilding, N.; Guzzo, C.; Xia, Y.; Zhou, B.; Li, S.; Dooley, L. T.; Goldstein, N. H.; Menter, A.; Group, A. S.. Comparison of Ustekinumab and Etanercept for Moderate-to-Severe Psoriasis. *N. Engl. J. Med.* **2010**, *362*, 118–128.

(45) Gordon, K. B.; Blauvelt, A.; Papp, K. A.; Langley, R. G.; Luger, T.; Ohtsuki, M.; Reich, K.; Amato, D.; Ball, S. G.; Braun, D. K.; Cameron, G. S.; Erickson, J.; Konrad, R. J.; Muram, T. M.; Nickoloff, B. J.; Osuntokun, O. O.; Secrest, R. J.; Zhao, F.; Mallbris, L.; Leonardi, C. L.; et al. Phase 3 Trials of Ixekizumab in Moderate-to-Severe Plaque Psoriasis. *N. Engl. J. Med.* **2016**, *375*, 345–356.

(46) Langley, R. G.; Elewski, B. E.; Lebwohl, M.; Reich, K.; Griffiths, C. E.; Papp, K.; Puig, L.; Nakagawa, H.; Spelman, L.; Sigurgeirsson, B.; Rivas, E.; Tsai, T. F.; Wasel, N.; Tying, S.; Salko, T.; Hampele, I.; Notter, M.; Karpov, A.; Helou, S.; Papavassilis, C.; et al. Secukinumab in Plaque Psoriasis—Results of Two Phase 3 Trials. *N. Engl. J. Med.* **2014**, *371*, 326–338.

(47) Bachelez, H.; van de Kerkhof, P. C.; Strohal, R.; Kubanov, A.; Valenzuela, F.; Lee, J. H.; Yakusevich, V.; Chimenti, S.; Papacharalambous, J.; Proulx, J.; Gupta, P.; Tan, H.; Tawadrous, M.; Valdez, H.; Wolk, R.; Investigators, O. P. T. C.. Tofacitinib *versus* Etanercept or Placebo in Moderate-to-Severe Chronic Plaque Psoriasis: a Phase 3 Randomised Non-Inferiority Trial. *Lancet* **2015**, *386*, 552–561.

(48) Garber, K. Psoriasis: From Bed to Bench and Back. *Nat. Biotechnol.* **2011**, *29*, 563–566.

(49) Kim, P.; Puoris'haag, M.; Cote, D.; Lin, C. P.; Yun, S. H. *In vivo* Confocal and Multiphoton Microendoscopy. *J. Biomed. Opt.* **2008**, *13*, 010501.

(50) Belsey, N. A.; Garrett, N. L.; Contreras-Rojas, L. R.; Pickup-Gerlaugh, A. J.; Price, G. J.; Moger, J.; Guy, R. H. Evaluation of Drug Delivery to Intact and Porated Skin by Coherent Raman Scattering and Fluorescence Microscopies. *J. Controlled Release* **2014**, *174*, 37–42.

(51) Kim, J. H.; Choi, Y. J.; Lee, B. H.; Song, M. Y.; Ban, C. Y.; Kim, J.; Park, J.; Kim, S. E.; Kim, T. G.; Park, S. H.; Kim, H. P.; Sung, Y. C.; Kim, S. C.; Shin, E. C. Programmed Cell Death Ligand 1 Alleviates Psoriatic Inflammation by Suppressing IL-17A Production from Programmed Cell Death 1-High T Cells. *J. Allergy Clin. Immunol.* **2016**, *137*, 1466–1476.